

## Article

# The Influence of Iron Tailings Powder on the Properties on the Performances of Cement Concrete with Machine-Made Sand

Lin Wang <sup>1,\*</sup>, Genkun Du <sup>1</sup>, Xinxin He <sup>1</sup>, Zicheng Wei <sup>1</sup>, Yubo Xu <sup>1</sup>, Shuai Li <sup>2</sup> and Xuejuan Liu <sup>2</sup>

<sup>1</sup> School of Civil and Transportation Engineering, Beijing University of Civil Engineering and Architecture, Beijing 100044, China; 2108590021014@stu.bucea.edu.cn (G.D.); 2108590020135@stu.bucea.edu.cn (X.H.); 2108590020129@stu.bucea.edu.cn (Z.W.); 2108590022112@stu.bucea.edu.cn (Y.X.)

<sup>2</sup> The First Civil Engineering Co., Ltd. of Crec Shanghai Group, Wuhu 241005, China; lszzfg931@163.com (S.L.); 18655378664@163.com (X.L.)

\* Correspondence: wanglin1@bucea.edu.cn

**Abstract:** Iron tailings powder (ITP) is a kind of solid waste, which pollutes the environment, without any treatment. The application of ITP in cement concrete is a good choice. In this study, the influence of ITP on the flowability, compressive strength, chloride ion permeability and the attenuation of the performance of cement concrete during freeze–thaw cycle (F-T) damage are investigated. An X-ray diffraction, an analysis of the pores and a scanning electron microscope (SEM) are obtained to analyze the mechanism of cement concrete’s performance. The results show that the addition of ITP can decrease the flowability of fresh cement concrete. Cement concrete with a 7% ITP to mass ratio of the total aggregate shows the highest compressive strength and the minimum chloride ion permeability. The relative dynamic modulus of the elasticity of the specimens with 7% ITP during the F-T is the highest. The corresponding mass loss rate is the lowest. The mercury intrusion analysis results show that the pore volume of the specimens with 7% ITP is the lowest. The SEM results confirm that the specimens with 7% ITP show the densest microstructures.

**Keywords:** iron tailings powder; flowability; compressive strength; chloride ion permeability; X-ray diffraction



**Citation:** Wang, L.; Du, G.; He, X.; Wei, Z.; Xu, Y.; Li, S.; Liu, X. The Influence of Iron Tailings Powder on the Properties on the Performances of Cement Concrete with Machine-Made Sand. *Coatings* **2023**, *13*, 946. <https://doi.org/10.3390/coatings13050946>

Academic Editor: Andrea Nobili

Received: 12 April 2023

Revised: 9 May 2023

Accepted: 15 May 2023

Published: 18 May 2023



**Copyright:** © 2023 by the authors. Licensee MDPI, Basel, Switzerland. This article is an open access article distributed under the terms and conditions of the Creative Commons Attribution (CC BY) license (<https://creativecommons.org/licenses/by/4.0/>).

## 1. Introduction

With the progress of industrialization worldwide, a large amount of metal tailings continuously accumulate in the environment [1,2]. Tailings storage not only occupies land resources and pollutes the environment, but also has potential safety hazards [3–5]. The main minerals in metal tailings are silicate minerals (quartz and feldspar), whose chemical components are mainly SiO<sub>2</sub>, Al<sub>2</sub>O<sub>3</sub> and Fe<sub>2</sub>O<sub>3</sub> [6–8].

Cement-based materials have been used in engineering for several years. The manufacturing of cement can require a large amount of energy and resources [9]. The mass production and use of cement not only consumes a large amount of energy and resources, but also causes ecological damage and environmental pollution [10–12]. Aimed at these issues, new cementitious materials need to be used to replace cement materials.

Young et al. [3] have reported that iron tailings can replace a part of clay raw material components. The presence of silicon and aluminum components in iron tailings has been shown to enhance the burnability of raw materials. This results in a reduction in the firing temperature of clinker minerals, which in turn leads to an improvement in the firing quality and hydration performance of clinker. Almada et al. [13,14] point out that iron tailings can optimize the pore structure of mortar, leading to improving the compactness of cement mortar, thus improving the corresponding mechanical strengths and durability. Pu [15] has prepared the iron tailings with a pozzolanic effect, and the iron tailings can promote the secondary hydration of aluminates in cement and significantly improve the gelling activity. The application of iron tailings in cement concrete can effectively increase the mechanical

strength of cement concrete [16,17]. Additionally, the permeability and frost resistance of cement concrete can be improved by mixing with the iron tailings [18,19]. Moreover, as reported in [20,21], iron tailings powder (ITP) can increase the amount of hydration products and optimize the pore size of concrete samples.

The fineness of the iron tailings can affect the mechanical strength and long-term performance. In order to solve the above problems, it is necessary to grind the iron tailings so the chemical treatment can be carried out. Mechanical grinding not only reduces particle size of the iron tailings, but also increases their specific surface area. Ultrafine iron tailings powder (ITP) may be advantageous in improving the properties of cement concrete [22,23]. However, few researchers have been attracted to the influence of ultrafine iron tailings on the fluidity, the mechanical performance and the durability of cement concrete.

In this study, the compressive strength, the chloride ion permeability and the freeze–thaw cycles (F-T) of cement concrete with ultrafine iron tailings are studied. The SEM photos, the XRD curves and the mercury intrusion curves have been obtained to reveal the mechanism of concrete performance with iron tailings.

## 2. Materials and Methods

### 2.1. Raw Materials

The applied cement in this research is ordinary Portland cement, provided by Beijing Jinyu Group Co., Ltd., Beijing, China. The compressive strength grade is 42.5 MPa. The grade II fly ash made by Beijing Jingyeda New Building Materials Co., Ltd., Beijing, China, and S95 blast furnace slag powder offered by Jintaicheng Technology Group Co., Ltd., Xingtai, China, are used as mineral admixtures. ITP was produced by grinding and sieving iron tailings mother rock. The iron tailings mother rock was supplied by the China Railway Shanghai Engineering Bureau in Shanghai, China. The ITP is shown in Figure 1.



**Figure 1.** The ITP.

Tables 1–3 show the chemical composition, particle passing percentage and technical index of cementitious material, respectively.

**Table 1.** Chemical composition (%).

Types	CaO	SiO <sub>2</sub>	Al <sub>2</sub> O <sub>3</sub>	Fe <sub>2</sub> O <sub>3</sub>	MgO	SO <sub>3</sub>	f-CaO	Loss	Others
Cement	61.30	22.41	6.95	3.41	2.62	2.86	/	/	0.45
Fly ash	2.90	51.24	34.12	4.23	0.62	1.21	0.54	1.83	/
Blast furnace slag	36.21	33.21	17.32	0.84	9.34	2.82	0.019	0.89	0.014
ITP	10.75	46.24	12.5	18.44	4.51	/	/	/	7.56

**Table 2.** Particle passing percentage of cementitious materials (%).

Types	0.3 $\mu\text{m}$	0.6 $\mu\text{m}$	1 $\mu\text{m}$	4 $\mu\text{m}$	8 $\mu\text{m}$	16 $\mu\text{m}$	32 $\mu\text{m}$	64 $\mu\text{m}$
Cement	0	0.79	3.37	18.17	33.42	48.74	70.28	90.45
Fly ash	0	0.28	1.05	7.34	17.91	31.80	55.51	82.24
Blast furnace slag	0	0.98	2.77	15.25	32.60	58.85	89.24	95.47
ITP	0	0.18	1.90	15.10	32.04	52.74	83.08	98.09

**Table 3.** Technical index.

Types	Fineness /(%)	Density/(g/cm <sup>3</sup> )	Water Demand Ratio /(%)	Mobility Ratio/(%)	Specific Surface Area/(m <sup>2</sup> /kg)	Burning Loss/(%)	Setting Time (min)	
							Initial Setting	Final Setting
Cement	/	3.1	/	/	390	/	220	255
Fly ash	10.2	2.21	98	/	385	/	/	/
Blast furnace slag	3.47	2.85	/	96	450	/	/	/
ITP	/	2.83	/	/	842	/	/	/

## 2.2. Test Apparatus

The vibratory ultra-micro crushing and grinding mixer, the HJW-60 concrete mixer and the slump bucket were produced by Jinan Henglongda Electromechanical Technology Co., Ltd., Jinan, China, Cangzhou Yixuan Test Instrument Co., Ltd., Cangzhou, China and Hebei Jingke Instrument Technology Co., Ltd., Cangzhou, China, respectively, while the YAW-3000 microcomputer controlled electro-hydraulic servo pressure testing machine, the NEL-PDU type chloride ion diffusion coefficient tester and the NJ-BSJ intelligent vacuum saturation machine were provided by Shanghai Sansi Zongheng Machinery Manufacturing Co., Ltd., Shanghai, China, Beijing Neerde Instrument Equipment Co., Ltd., Beijing, China and Cangzhou Huaheng Test Instrument Co., Ltd., Cangzhou, China, individually. Additionally, the CDR6-9 fully automatic concrete rapid freeze–thaw test equipment, the DT-10 concrete dynamometer and the ZEISS GeminiSEM 300 scanning electron microscope were offered by Beijing Yanke New Technology Corporation, Beijing, China, Tianjin Zhongshi Technology Instrument Co., Ltd., Tianjin, China and Carl Zeiss (Shanghai) Management Co., Ltd., Shanghai, China, respectively. The X'Pert PRO MPD type X-ray diffraction pattern analyzer and the MicroActive Auto Pore AutoPore IV9510 high-performance fully automatic mercury intrusion meter were made by Panalytical Company in the Netherlands and McMurray Tec (Shanghai) Instrument Co., Ltd., Shanghai, China, respectively.

## 2.3. Specimens Manufacturing and Measurement

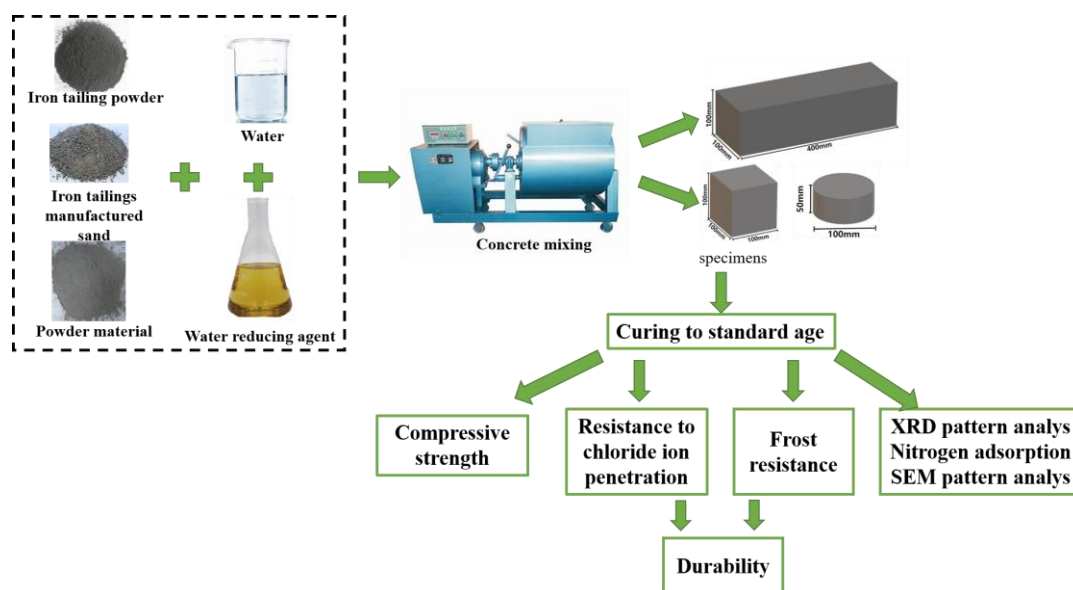
### 2.3.1. Specimens Manufacturing

The specimens were made with the mixing proportions in Table 4. The manufacturing process is described in these steps. The ITP content ranged from 0% to 15% of the total mass of the total binder materials.

All powdered materials were stirred in the HJW-60 concrete mixer with a mixing speed of 48 r/min for 1 min. Then, the coarse aggregate was added and mixed with the same stirring speed for another 1 min. Finally, the mixed solution (water and water reducing agent) was mixed in the concrete mixer with a speed of 48 r/min for the last 2 min. The manufacturing process is shown in Figure 2.

**Table 4.** The proportions of concrete mix.

Cement (kg/m <sup>3</sup> )	Fly Ash (kg/m <sup>3</sup> )	Mineral Powder (kg/m <sup>3</sup> )	ITP Content/%	ITP (kg/m <sup>3</sup> )	Stone (kg/m <sup>3</sup> )	Manufactured Sand (kg/m <sup>3</sup> )	Water (kg/m <sup>3</sup> )	Water Reducer (%)
208	105	105	0	0	1077	780	176	0.5
208	105	105	3	13	1077	780	176	0.5
208	105	105	5	21	1077	780	176	0.5
208	105	105	7	29	1077	780	176	0.5
208	105	105	9	38	1077	780	176	0.5
208	105	105	11	46	1077	780	176	0.5
208	105	105	13	54	1077	780	176	0.5
208	105	105	15	63	1077	780	176	0.5
100	50	50	0	0	0	0	84	1
100	50	50	5	10	0	0	84	1
100	50	50	7	14	0	0	84	1

**Figure 2.** The productive process of sample.

### 2.3.2. Measurement of Slump

Slump bucket was used for determining the slump of fresh cement concrete. The fresh cement concrete was poured into the slump bucket at three steps. When the pouring was finished, the slump bucket was pulled vertically, and the slump of fresh cement concrete was measured referring to the Chinese standard GB/T50080-2016 [24].

### 2.3.3. Measurement of Compressive Strength

Specimens with size of  $100 \times 100 \times 100 \text{ mm}^3$  were used for the measurement of compressive strength referring to the Chinese standard GB/T50081-2019 [25]. All specimens were cured in the standard curing room ( $20 \pm 2 \text{ }^\circ\text{C}$  and a relative humidity of 98.2%) for 3 days, 7 days and 28 days. The compressive strength of concrete was tested using the YAW-3000 microcomputer controlled electro-hydraulic servo pressure testing machine.

### 2.3.4. Measurement of Chloride Ion Permeability and Freeze-Thaw Resistance

Electric flux method was used to test the chloride ion permeability. The specimens used in this experiment show a size of  $\Phi 100 \text{ mm} \times 50 \text{ mm}$ . NEL-PDU type chloride ion diffusion coefficient tester was used for the determination of electric flux. Before the measurement of electric flux, a vacuum water saturation treatment was carried out on all specimens with a NJ-BSJ intelligent vacuum saturation machine.

Specimens with a size of  $100 \times 100 \times 400 \text{ mm}^3$  were used for the experiments of freeze–thaw cycles. CDR6-9 fully automatic concrete rapid freeze-thaw test equipment

was applied in the measurement of freeze–thaw (F-T) cycles. The freeze–thaw temperature ranged from  $-15\text{ }^{\circ}\text{C}$  to  $8\text{ }^{\circ}\text{C}$ . The specimens were immersed in the rubes filled with water. The relative dynamic elastic modulus (*RDEM*) was measured by DT-10 concrete dynamometer. The mass and relative dynamic elastic modulus were tested, each at 25 freeze–thaw cycles. Three specimens of each group were used for every experiment. All the experiments were carried out according to the GB/T 50082-2009 Chinese standard [26], as shown in Figure 3.

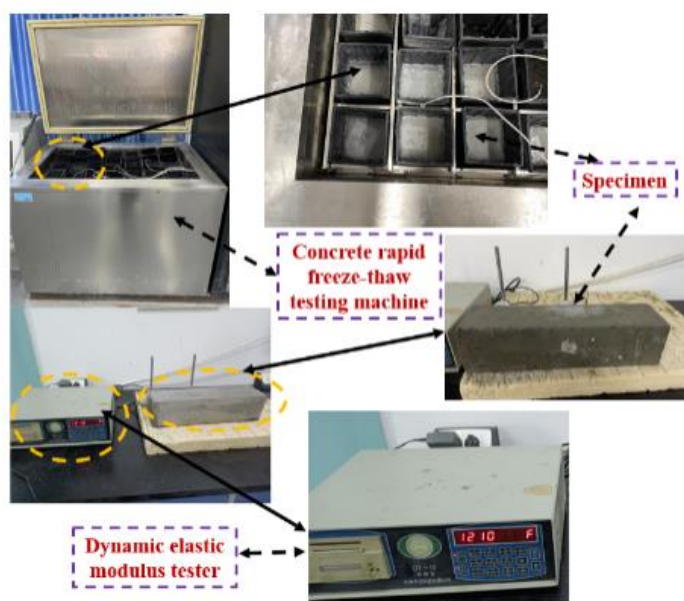


**Figure 3.** The measuring process of freeze–thaw experiment.

### 2.3.5. Measurement of Microscopic Performance

The samples were immersed in alcohol for 4 days. Then, all samples were dried in the vacuum drying oven at a temperature of  $60\text{ }^{\circ}\text{C}$  for 4 days. After that, the samples sprayed with gold, with the maximum diameter of 0.2 cm, were used for the SEM experiment by ZEISS GeminiSEM 300 scanning electron microscope. The dried samples were used for the measurement of XRD by X'Pert PRO MPD type X-ray diffraction pattern analyzer. The tested samples were ground and screened by utilizing a square mesh sieve. The side length of each aperture was 75  $\mu\text{m}$ . The internal parts of the samples whose maximum diameter was 0.5 mm were used for the mercury intrusion analysis with MicroActive Auto Pore AutoPore IV9510 high-performance fully automatic mercury intrusion meter.

## 3. Results and Discussion

### 3.1. The Slump of Fresh Cement Concrete

The slump of fresh cement concrete is shown in Figure 4. The slump of fresh cement concrete decreased with the increasing dosages of ITP. The minimum slump of fresh cement concrete was 210 mm. When the addition of ITP increased from 0% to 15%, the decreasing rate of slump was 13.7%. This is attributed to the fact that the ITP showed a higher specific surface area than the cement. The total specific surface area was increased by adding the ITP. Therefore, more free water was absorbed by the ITP and the slump was decreased. The decreasing rate of the slump fits the equation of  $D_r = 1.89 + 2.56\sin(\pi(C_i + 1.27)/3.58)$ , where  $D_r$  is the decreasing rate and  $C_i$  is the mass ratio of the ITP.

### 3.2. The Compressive Strength

The compressive strength of cement concrete with different dosages of ITP is shown in Figure 5. The compressive strength of cement concrete increased when the dosages of ITP increased from 0% to 7%, which was ascribed to the fact that the ITP showed

a higher specific surface area than the cement. The ITP filled the pores between the particles of the cementitious material and optimized the particle grading of the cementitious material [27–29], which reduced the porosity of the concrete and made the concrete more dense. Therefore, the compressive strength was improved by adding the ITP. However, when the content of ITP was higher than 7%, the compressive strength decreased with the increasing dosage of ITP due to the fact that an excessive amount of ITP can damage the optimized particle grading and reduce the compactness of the concrete, leading eventually to a decrease in the compressive strength of cement concrete. In addition, when the amount of ITP is too high, some of the ITP will exist in a free state. This part of ITP is disadvantageous for the formation of cement paste or interface transition zone [30,31]. Consequently, the compressive strength is decreased. Finally, as can be found in Figure 5, the compressive strength increased with the increasing curing age, which was attributed to the improved hydration degree. The growth rate of the mechanical strengths fit the equation of sine function with the mass ratio of the ITP. The compressive strengths of cement concrete with 7% ITP were 13%, 11.7% and 9.6% higher than the specimens without ITP. The compressive strength of cement concrete increased with the increasing curing ages due to the improved hydration process.

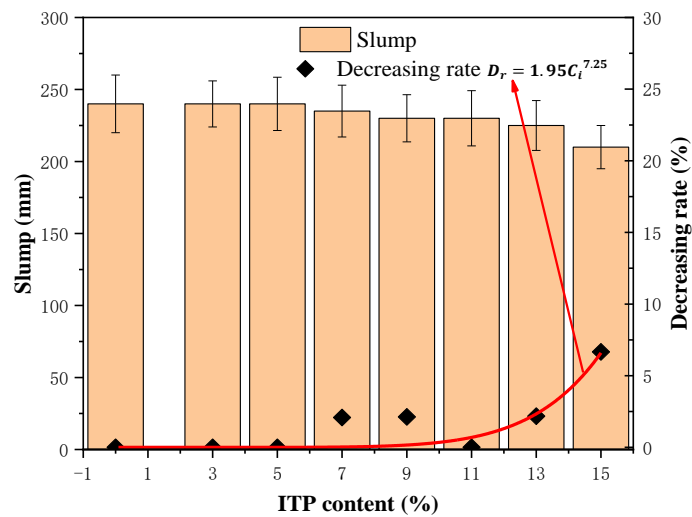


Figure 4. Slump of fresh concrete mixed with ITP.

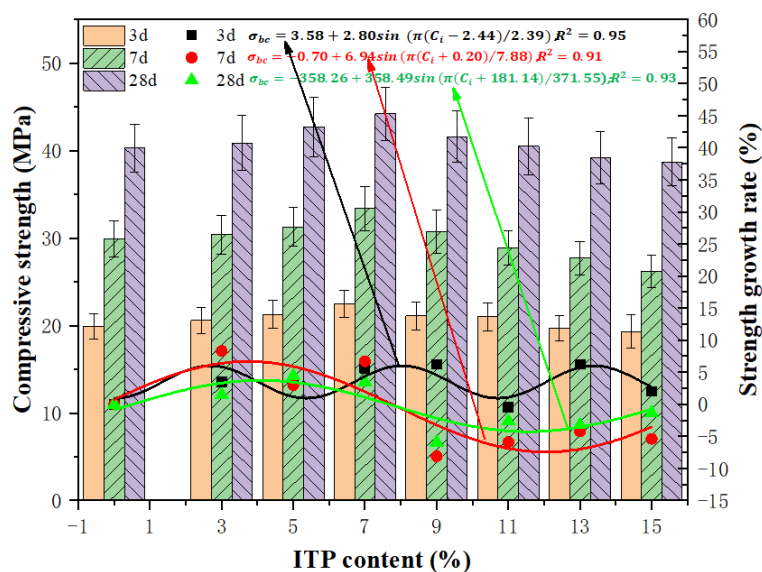
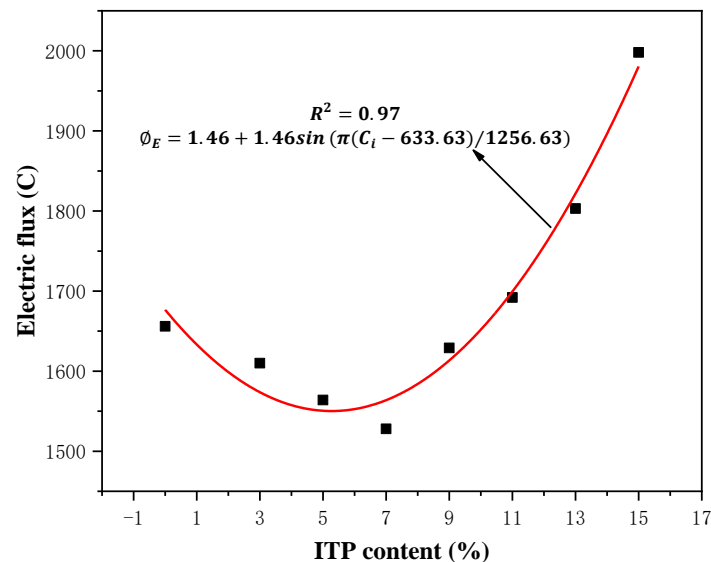


Figure 5. Compressive strength of concrete mixed with ITP.

### 3.3. The Durability

As described in the Chinese standard, the GB/T 50082-2009 [26], the electric flux of cement concrete is used for reflecting the chloride ion permeability. In this study, this parameter was used to represent the chloride ion permeability. The electric flux of cement concrete with powder is shown in Figure 6. As observed in Figure 6, the electric flux shows a downward trend with the dosage of ITP ranging from 0% to 7%, showing the increasing resistance to chloride ion permeability. However, when the dosage of ITP increased from 7% to 15%, the electric flux increased with the increasing content ITP, which indicates the lower permeability of resistant chloride ions. This is attributed to the microaggregate effect [32–34], which effectively fills the pores inside the concrete and improves the pore structure concrete. Therefore, the compactness was increased, leading to a reduction in the chloride ion diffusion channels and an increase in the resistance to chloride ions' permeability. However, when the dosage of ITP was higher than 7%, the activity of hydraulic substances was reduced by adding the ITP. Hence, the chloride ion impermeability was increased by the increasing dosages of ITP. The change in the electric flux fits the equation of  $\Phi_E = 1.46 + 1.46\sin(\pi(C_i - 633.63)/1256.63)$ , where  $\Phi_E$  is the change in the electric flux and  $C_i$  is the mass ratio of the ITP.



**Figure 6.** Variation curve of concrete electric flux with the amount of ITP.

The mass loss rates and the relative dynamic modulus of elasticity of cement concrete are shown in Figure 7. As depicted in Figure 7, the mass loss rates increased with the increasing number of F-T. Moreover, the relative dynamic modulus of elasticity decreased during the F-T. This is ascribed to the fact that the freeze–thaw action can increase the inner cracks of the cement concrete [35,36]. Therefore, mass was decreased by the increasing number of F-T. The increased inner cracks by F-T can block transmitting of sound, leading to a decrease in the relative dynamic elastic modulus of the samples. When the mass ratio of ITP was lower than 7%, the relative dynamic elastic modulus were increased and the mass loss rate were decreased with the increasing dosages of ITP, due to the increased compactness by ITP. While, when the dosages of ITP were higher than 7%, the relative dynamic elastic modulus was decreased and mass loss rate was increased with the increasing dosage of ITP. The decreasing rate of the relative dynamic modulus of elasticity ( $RDEM$ ) fits the equation of  $RDEM = 281.9N^{0.3}$ ;  $RDEM = 220.7N^{0.2}$ ;  $RDEM = 220.7N^2$ ;  $RDEM = 217.0N^{-0.2}$ ;  $RDEM = 249.1N^{-0.3}$ , and the growth rate of the mass loss rate ( $\Delta m/m$ ) fits the equation of power function (where  $RDEM$  is the relative dynamic elastic modulus;  $\Delta m/m$  is the mass ratio of the ITP; and  $N$  is the number of F-T).

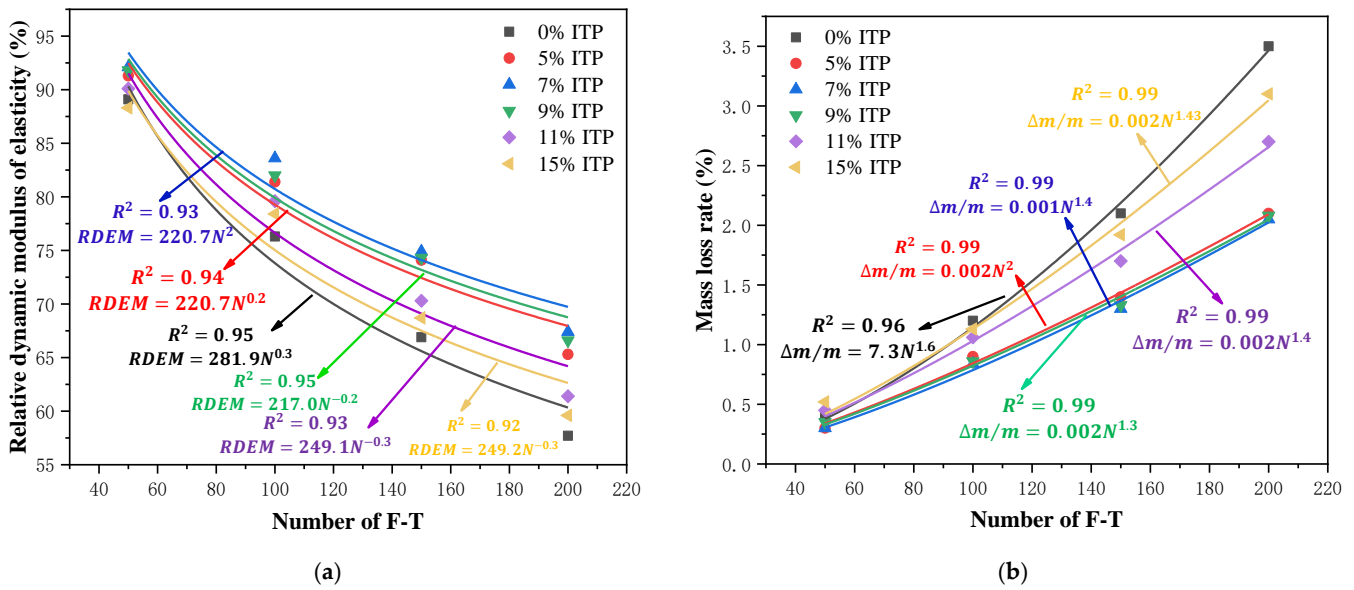


**Figure 7.** The relative dynamic elastic modulus and mass loss rate of concrete with the number of F-T. (a) Relative dynamic elastic modulus; (b) Mass loss rate.

3.4. The Microanalysis

The SEM photos of iron tailings are illustrated in Figure 8. The iron tailings are composed of small spherical particles and irregular sheet-like structures that exhibit an obvious agglomeration phenomenon, mainly consisting of powder particles as the skeleton. Small mineral particles adhere to each other and accumulate to form an agglomeration structure. The surface of the particles generally exhibits irregular edges and corners, which allows for a better filling of the pore spaces between cement-based material particles due to their small size. As a result, iron tailings can be used to enhance the compactness of cement-based materials, thereby improving their mechanical strength and resistance to chloride ion permeability.

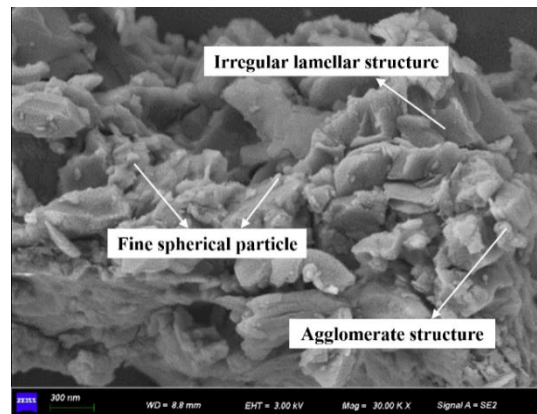


**Figure 8.** Apparent structure of ITP.

Figure 9 displays the particle size distributions of both cement and iron tailings. The particle sizes of iron tailings ranged between 24 μm and 40 μm. Notably, the particle size distribution curve of iron tailings was narrower than that of cement particles [34].

Figure 10 shows the XRD curves of the specimens, revealing the presence of quartz, annite, actinolite, cordierite, and CaSO<sub>3</sub>. The chemical compounds of iron tailings are ranked in the following order: SiO<sub>2</sub>, Fe<sub>2</sub>O<sub>3</sub>, Al<sub>2</sub>O<sub>3</sub>, CaO and MgO. Therefore, adding iron tailings can effectively increase the hydration degree of cement, ultimately enhancing the compactness of the concrete and improving its mechanical strength and durability.

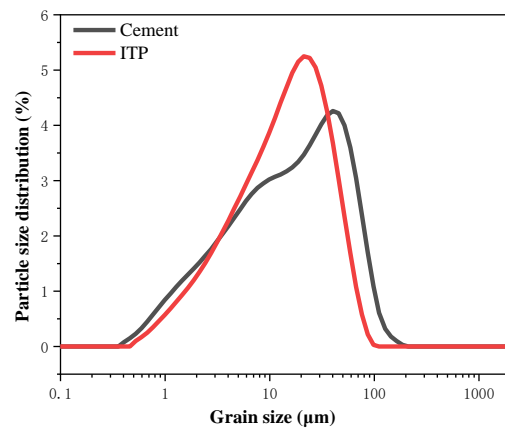


Figure 9. Particle size distribution curve.

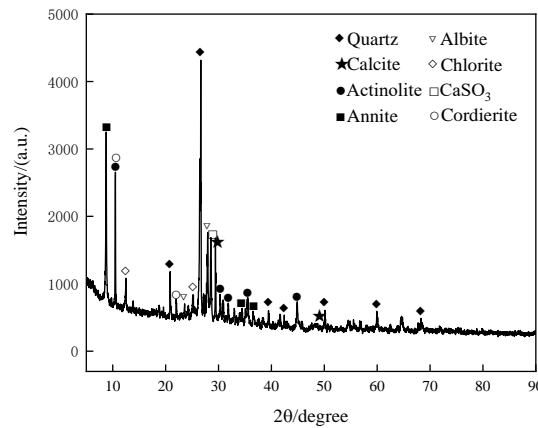


Figure 10. The XRD curves of the specimen.

Figure 11 displays the X-ray spectrum of cement concrete specimens with ITP. The diffraction peaks of ettringite,  $3\text{CaO}\cdot\text{SiO}_2$ ,  $2\text{CaO}\cdot\text{SiO}_2$ ,  $\text{SiO}_2$  and  $\text{Ca}(\text{OH})_2$  were observed. As the dosage of ITP increased, the diffraction peaks of  $\text{Ca}(\text{OH})_2$  and ettringite decreased. This is because as the amount of iron tailings increased, the water-cement ratio decreased, resulting in less water being required for the hydration of other cementitious materials. This, in turn, delayed the early hydration process of the cement. Moreover, the diffraction peaks of  $\text{SiO}_2$  and  $2\text{CaO}\cdot\text{SiO}_2$  increased, indicating that ITP has an inhibitory effect on the early hydration of cement. As a result, the diffraction peaks of  $\text{SiO}_2$  and  $2\text{CaO}\cdot\text{SiO}_2$  increased with increasing ITP content.

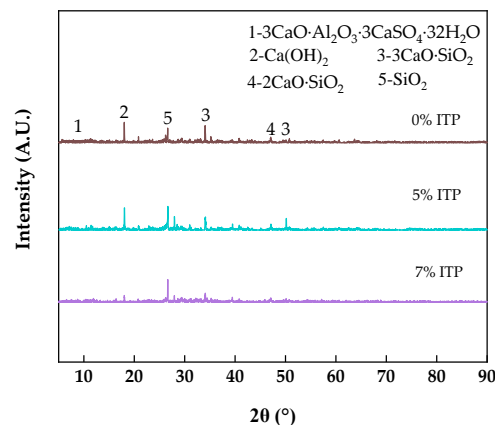
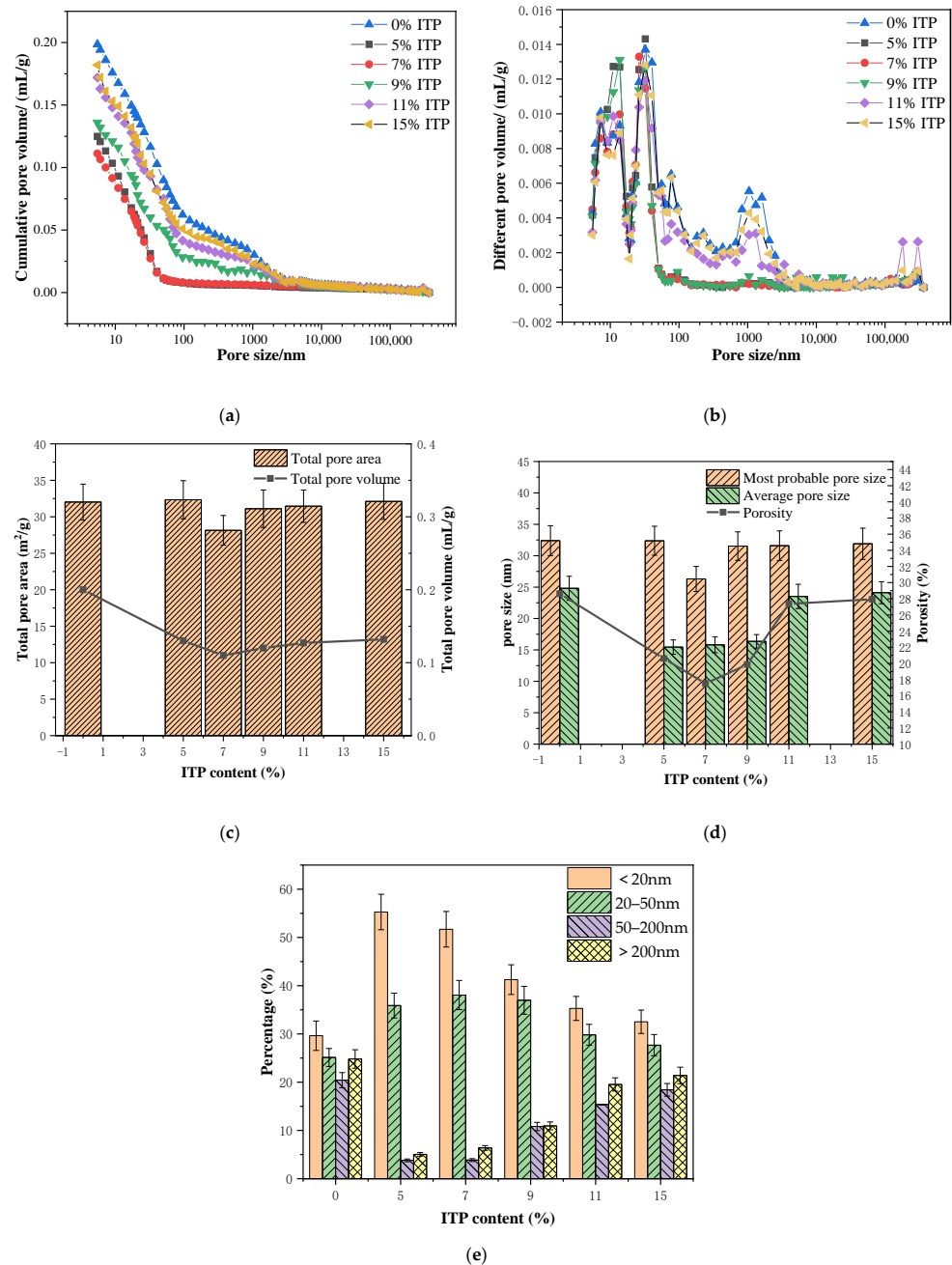


Figure 11. The XRD spectrum of cement concrete specimens with ITP.

Figure 12 shows the mercury intrusion curves, indicating the pore diameter ranges of cement concrete to be 0–50 nm, 0–20 nm, 0–20 nm, 0–50 nm and 0–50 nm. As the dosage of ITP increased, the total volume of pores in cement concrete decreased due to the physical filling effect of ITP [37–39]. As a result, the structure of the cement stone was improved and porosity was reduced, leading to a more compact cement stone.



**Figure 12.** Effect of incorporation of ITP on the pore structure of net cement paste. (a) Different pore volume; (b) Cumulative pore volume; (c) Total pore volume and total pore area; (d) Most probable pore size, average pore size and porosity; (e) Pore size distribution.

Figure 13 displays SEM photos of specimens with varying ITP dosages, ranging from 0% to 15%. With 0% ITP, needle-shaped and flower-shaped hydration products were observed. These products were relatively large, but the morphology was loose, and obvious cracks could be observed at the interface transition zone. As shown in Figure 13a–d, when the mass ratio of ITP was less than or equal to 7%, the structure of the hydration products

was denser, resulting in an overall compact structure. The sufficient hydration of cement generated more needle-like products, which interwove to form a spatial network structure. The ITP particles in the structure served to fill the pores. However, as depicted in Figure 13f–h, when the mass ratio of ITP was higher than 7%, the compactness of the concrete structure decreased significantly with increasing mass ratio of ITP. At the same time, a large amount of micro powder attached to the surface of hydration products, resulting in the generation of a large amount of gel-like structure. Moreover, the micro powder was not effectively wrapped, leading to the existence of micro-cracks in the specimens, which negatively affected their mechanical strength.

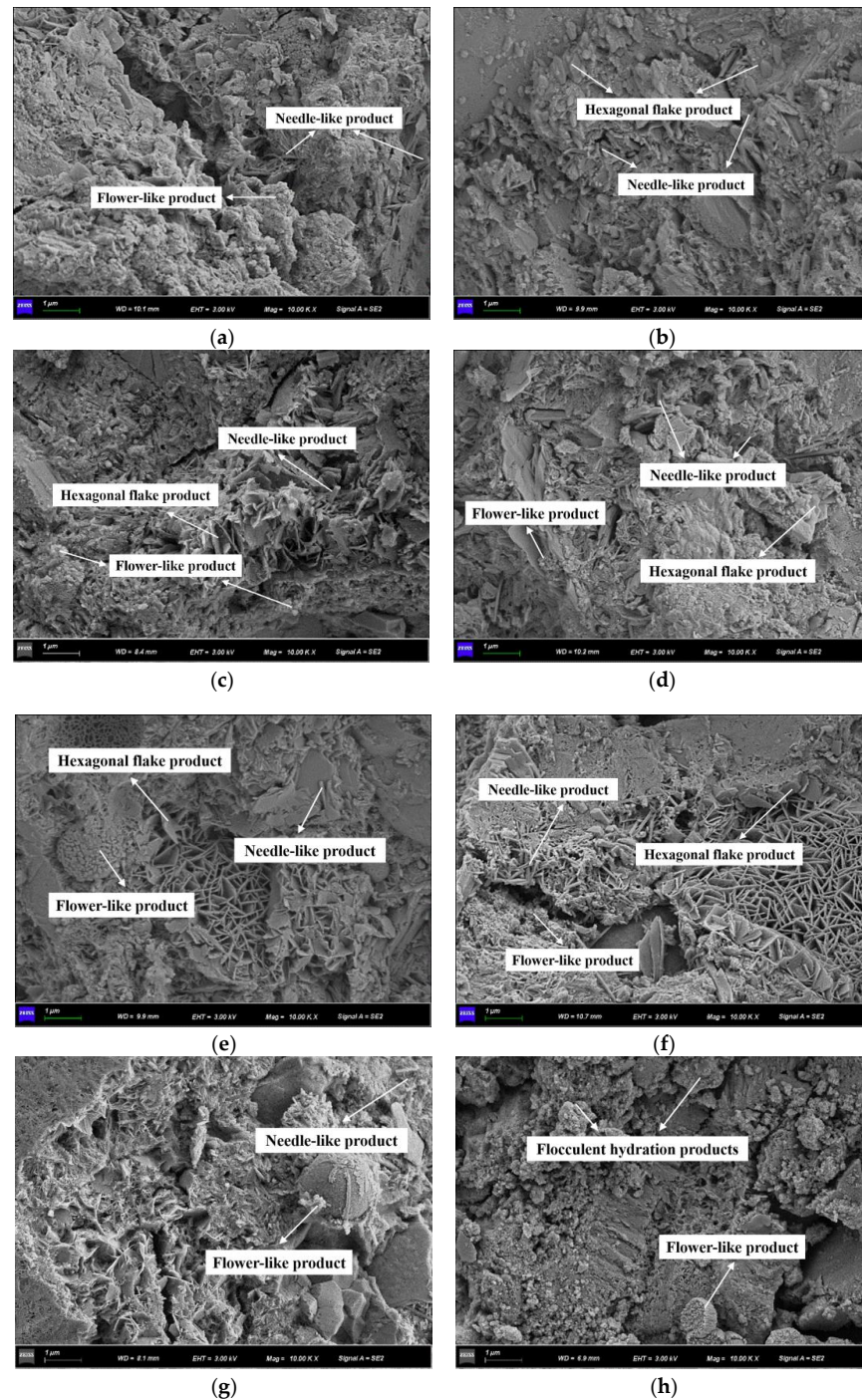


**Figure 13.** SEM microstructure photos of specimens. (a) 0% ITP; (b) 3% ITP; (c) 5% ITP; (d) 7% ITP; (e) 9% ITP; (f) 11% ITP; (g) 13% ITP; (h) 15% ITP.

#### 4. Conclusions

In this study, the effects of the addition of ITP on compressive strength, chloride ion permeability and freeze–thaw resistance were investigated. XRD, MIA and SEM were applied in analyzing the mechanism of the macro performance. The research results are summarized as follows.

(1) The flowability of fresh cement concrete was decreased with the higher replacement ratio of iron tailings powder. The relationship between concrete mixture slump loss and iron tailings powder dosage can be described by a power function formula.

(2) With the increasing replacement ratio of iron tailings powder, the compressive strength, chloride ion anti-permeability and freeze–thaw resistance presented a tendency of initial enhancement and later degradation.

(3) When the replacement ratio of ITP was 7%, the cement concrete showed the maximum compressive strength, the minimum chloride ion permeability and the best resistance of freeze–thaw cycles.

(4) The cement concrete incorporated with 7% iron tailings powder showed the optimal pore distribution and minimum total pore volume. At this dosage of iron tailings powder, the hydration products of cement concrete specimens was most compacted.

(5) The researching achievements have provided new ideas for handling solid waste.

**Author Contributions:** Conceptualization, L.W. and G.D.; methodology, X.H.; software, Z.W.; validation, L.W., G.D. and Y.X.; formal analysis, L.W.; investigation, X.L.; resources, X.H.; data curation, G.D.; writing—original draft preparation, L.W.; writing—review and editing, L.W.; visualization, S.L.; supervision, L.W.; project administration, G.D.; funding acquisition, L.W. All authors have read and agreed to the published version of the manuscript.

**Funding:** This research was funded by the Basic Research Funds For Municipal Colleges and Universities number (X18265) and the Research and Engineering Application of Iron Tailings Concrete (H22148), a Horizontal Project of Beijing University of Architecture.

**Institutional Review Board Statement:** Not applicable.

**Informed Consent Statement:** Not applicable.

**Data Availability Statement:** Not applicable.

**Conflicts of Interest:** The authors declare no conflict of interest.

#### References

1. Shettima, A.U.; Hussin, M.W.; Ahmad, Y.; Mirza, J. Evaluation of iron ore tailings as replacement for fine aggregate in concrete. *Constr. Build. Mater.* **2016**, *120*, 72–79. [[CrossRef](#)]
2. Chen, T.; Chang, L.; Yan, B.; Li, L.L.; Xu, D.M.; Ying, G.G. Spatial distribution and environmental implications of heavy metals in typical lead (Pb)-zinc (Zn) mine tailings impoundments in Guangdong Province, South China. *Environ. Sci. Pollut. Res.* **2018**, *25*, 36702–36711. [[CrossRef](#)] [[PubMed](#)]
3. Young, G.; Yang, M. Preparation and characterization of Portland cement clinker from iron ore tailings. *Constr. Build. Mater.* **2019**, *197*, 152–156. [[CrossRef](#)]
4. Piciullo, L.; Storøsten, E.B.; Liu, Z.Q.; Nadim, F.; Lacasse, S. A new look at the statistics of tailings dam failures. *Eng. Geol.* **2022**, *303*, 106657. [[CrossRef](#)]
5. Falagan, C.; Grail, B.M.; Johnson, D.B. New approaches for extracting and recovering metals from mine tailings. *Miner. Eng.* **2017**, *106*, 71–78. [[CrossRef](#)]
6. Carmignano, O.R.; Vieira, S.S.; Teixeira, A.P.C.; Lameiras, F.S.; Brandão, P.R.G.; Lago, R.M. Iron Ore Tailings: Characterization and Applications. *J. Braz. Chem. Soc.* **2021**, *32*, 1895–1911.
7. Yang, C.M.; Cui, C.; Qin, J.; Cui, X.Y. Characteristics of the fired bricks with low-silicon iron tailings. *Constr. Build. Mater.* **2014**, *70*, 36–42. [[CrossRef](#)]
8. Fontes, W.C.; Carvalho, J.M.F.D.; Andrade, L.C.R.; Segadaes, A.M.; Peixoto, R.A.F. Assessment of the use potential of iron ore tailings in the manufacture of ceramic tiles: From tailings-dams to “brown porcelain”. *Constr. Build. Mater.* **2019**, *206*, 111–121. [[CrossRef](#)]
9. Supino, S.; Malandrino, O.; Testa, M.; Sica, D. The manufacturing of cement can cost large amount of energy and resources. *J. Clean. Prod.* **2016**, *112*, 430–442. [[CrossRef](#)]

10. Khan, R.; Jabbar, A.; Ahmad, I.; Khan, W.; Khan, A.N.; Mirza, J. Reduction in environmental problems using rice-husk ash in concrete. *Constr. Build. Mater.* **2012**, *30*, 360–365. [[CrossRef](#)]
11. Naik, T.R. Sustainability of Concrete Construction. *Pract. Period. Struct. Des. Constr.* **2008**, *13*, 98–103. [[CrossRef](#)]
12. Vieira, D.R.; Calmon, J.L.; Coelho, F.Z. Life cycle assessment (LCA) applied to the manufacturing of common and ecological concrete: A review. *Constr. Build. Mater.* **2016**, *124*, 656–666. [[CrossRef](#)]
13. Almada, B.S.; Melo, H.S.S.; Duarte, M.S.; Aguilar, M.T.P.; Garcia, D.C.S.; Silva, G.J.B.; Santos, W.J. Study of mechanical, durability and microstructural properties of cementitious composite with addition of different iron ore tailings from Brazil. *J. Mater. Res. Technol.* **2022**, *18*, 1947–1962. [[CrossRef](#)]
14. Zhang, W.F.; Gu, X.W.; Qiu, J.P.; Liu, J.P.; Zhao, Y.Q.; Li, X.H. Effects of iron ore tailings on the compressive strength and permeability of ultra-high performance concrete. *Constr. Build. Mater.* **2020**, *260*, 119917. [[CrossRef](#)]
15. Pu, C.A. Study on the Activation Process and Mechanism of Iron Tailings Powder and its Influence on the Performance of Concrete. Ph.D. Thesis, China University of Mining & Technology, Beijing, China, 2018.
16. Chen, Z.; Chen, S.L.; Zhou, Y.W.; Zhang, C.Y.; Meng, T.T.; Jiang, S.S.; Liu, L.W.; Hu, G.Q. The application of iron tailings in cement concrete can effectively increase the mechanical strength of cement concrete. *Constr. Build. Mater.* **2022**, *338*, 127584. [[CrossRef](#)]
17. Sushmitha, K.S.; Dhanabal, P. Study on Properties of Concrete with Iron Ore Tailing and Glass Waste. *J. Mod. Mater.* **2021**, *8*, 30–39. [[CrossRef](#)]
18. Adiguzel, D.; Tuylu, S.; Eker, H. Utilization of tailings in concrete products: A review. *Constr. Build. Mater.* **2022**, *360*, 129574. [[CrossRef](#)]
19. Mishra, O.; Singh, S.P. An overview of microstructural and material properties of ultra-high-performance concrete. *J. Sustain. Cem.-Based Mater.* **2019**, *8*, 97–143. [[CrossRef](#)]
20. Protasio, F.N.M.; Avillez, R.R.D.; Letichevsky, S.; Silva, F.D.A. The use of iron ore tailings obtained from the Germano dam in the production of a sustainable concrete. *J. Clean. Prod.* **2021**, *278*, 123929. [[CrossRef](#)]
21. Carrasco, E.V.M.; Magalhaes, M.D.C.; Santos, W.J.D.; Alves, R.C.; Mantilla, J.N.R. Characterization of mortars with iron ore tailings using destructive and nondestructive tests. *Constr. Build. Mater.* **2017**, *131*, 31–38. [[CrossRef](#)]
22. Wu, R.D.; Zhang, Y.Y.; Zhang, G.T.; An, S.H. Enhancement effect and mechanism of iron tailings powder on concrete strength. *J. Build. Eng.* **2022**, *57*, 104954. [[CrossRef](#)]
23. Han, F.H.; Luo, A.; Liu, J.H.; Zhang, Z.Q. Properties of high-volume iron tailing powder concrete under different curing conditions. *Constr. Build. Mater.* **2020**, *241*, 118108. [[CrossRef](#)]
24. GB/T50080-2016; Standard for Test Method of Performance on Ordinary Fresh Concrete. General Administration of Quality Supervision, Inspection and Quarantine of the People's Republic of China: Beijing, China, 2016.
25. GB/T50081-2019; Standard for Test Method of Concrete Physical and Mechanical Properties. General Administration of Quality Supervision, Inspection and Quarantine of the People's Republic of China: Beijing, China, 2019.
26. GB/T50082-2009; Standard for Test Method of Long-Term Performance and Durability of Ordinary Concrete. General Administration of Quality Supervision, Inspection and Quarantine of the People's Republic of China: Beijing, China, 2009.
27. Cui, L.Y.; Chen, P.Y.; Wang, L.; Xu, Y.; Wang, H. Reutilizing Waste Iron Tailing Powders as Filler in Mortar to Realize Cement Reduction and Strength Enhancement. *Materials* **2022**, *15*, 541. [[CrossRef](#)] [[PubMed](#)]
28. Gupta, T.; Kothari, S.; Siddique, S.; Sharma, R.K.; Chaudhary, S. Influence of stone processing dust on mechanical, durability and sustainability of concrete. *Constr. Build. Mater.* **2019**, *223*, 918–927. [[CrossRef](#)]
29. Karakurt, C.; Dumangöz, M. Rheological and Durability Properties of Self-Compacting Concrete Produced Using Marble Dust and Blast Furnace Slag. *Materials* **2022**, *15*, 1795. [[CrossRef](#)]
30. Campos, H.F.; Rocha, T.M.S.; Reus, G.C.; Klein, N.S.; Klein, N.S.; Filho, J.M. Determination of the optimal replacement content of Portland cement by stone powder using particle packing methods and analysis of the influence of the excess water on the consistency of pastes. *Rev. IBRACON Estrut. Mater.* **2019**, *12*, 210–232. [[CrossRef](#)]
31. Muhit, I.B.; Raihan, M.T.; Nuruzzaman, M. Determination of mortar strength using stone dust as a partially replaced material for cement and sand. *Adv. Concr. Constr.* **2014**, *2*, 249–559. [[CrossRef](#)]
32. Xie, K.Z.; Bai, M.Y.; Qing, Z.G.; Li, J.; Ge, B.Z. Study on Durability of Manufactured Sand Based on Stone Powder Content. *Sci. Adv. Mater.* **2018**, *10*, 1608–1614. [[CrossRef](#)]
33. Han, F.H.; Li, L.; Song, S.M.; Liu, J.H. Early-age hydration characteristics of composite binder containing iron tailing powder. *Powder Technol.* **2017**, *315*, 322–331. [[CrossRef](#)]
34. Ma, Z.M.; Liu, M.; Duan, Z.H.; Liang, C.F.; Wu, H.X. Effects of active waste powder obtained from C&D waste on the microproperties and water permeability of concrete. *J. Clean. Prod.* **2020**, *257*, 120518.
35. Li, L.J.; Liu, Q.F.; Tang, L.P.; Hu, Z.; Wen, Y.; Zhang, P. Chloride penetration in freeze–thaw induced cracking concrete: A numerical study. *Constr. Build. Mater.* **2021**, *302*, 124291. [[CrossRef](#)]
36. Medina, C.; Rojas, M.L.S.; Frias, M. Freeze-thaw durability of recycled concrete containing ceramic aggregate. *J. Clean. Prod.* **2013**, *40*, 151–160. [[CrossRef](#)]
37. Yang, M.J.; Sun, J.H.; Dun, C.Y.; Duan, Y.J.; Meng, Z.L. Cementitious activity optimization studies of iron tailings powder as a concrete admixture. *Constr. Build. Mater.* **2020**, *265*, 120760. [[CrossRef](#)]

38. Han, F.H.; Zhang, H.B.; Liu, J.H.; Song, S.M. Influence of iron tailing powder on properties of concrete with fly ash. *Powder Technol.* **2022**, *398*, 117132. [[CrossRef](#)]
39. Eugenio, T.M.C.; Fagundes, J.F.; Viana, Q.S.; Vilela, A.P.; Mendes, R.F. Study on the feasibility of using iron ore tailing (iot) on technological properties of concrete roof tiles. *Constr. Build. Mater.* **2021**, *279*, 122484. [[CrossRef](#)]

**Disclaimer/Publisher's Note:** The statements, opinions and data contained in all publications are solely those of the individual author(s) and contributor(s) and not of MDPI and/or the editor(s). MDPI and/or the editor(s) disclaim responsibility for any injury to people or property resulting from any ideas, methods, instructions or products referred to in the content.